Scattering by cracks: Numerical simulations using a boundary finite element method.

Carlos J. S. Alves, Bruno Pereira, Pedro Serranho
Departamento de Matemática and *Centro de Matemática Aplicada,*
Instituto Superior Técnico,
Av. Rovisco Pais 1, 1049-001 Lisboa, Portugal

Abstract
We present several simulations of the amplitude scattered by acoustic cracks in the resonance region. The results are obtained with a boundary element method applied to a variational formulation derived from the double layer potential. Simulations on the far field patterns allow to characterize some information on the shape of the scattering obstacle. We include the case of non planar cracks in the three dimensional case, presenting several examples where it becomes clear the good convergence of the method. Moreover, we show that even with sparse meshes the method is able to give a global feature of the far field pattern of the scattered wave.

1 Introduction

Acoustic and elastic scattering by cracks is an old issue, with many applications in industrial problems, for instance, the detection of cracks in materials. Early works by Bouwkamp[5] and Jones[9], in the acoustic case, tried to solve this problem. In terms of integral equations, the difficulty is to express the exterior domain problem in terms of an integral equation with a non hypersingular kernel. First attempts considered only simple geometries, mainly penny-shaped flat cracks.

A way to deal with this problem was to use analytical series developments. This was done only many years later for the elastic penny-shaped crack by Martin and Wickham [10]. It was only afterwards that some techniques to regularize the problem (and then use collocation methods) were applied (eg.[11], [4]), but all numerical simulations available still dealt

with simple geometries and flat cracks. Based on a variational formulation method and the good numerical properties proved by Ha Duong [7], in [1] numerical simulations were first presented for plane cracks of arbitrary geometries and comparisons with previous methods were made. However, in [1], the method was restricted to flat cracks. Here, based on the variational formulation of Hamdi [8], we show our first results extending the method to the case of non flat cracks, but only in acoustic scattering.

The text is organized as follows. In the next section we state the problem and present the variational formulation, then we roughly describe the numerical procedure which is quite similar to the implementation of the finite element method in two dimensional problems and it was already used in [1]. In the last section we present several numerical examples and convergence tests that allow to conclude the good performance of the BFEM (boundary finite element method).

2 Scattering by acoustic cracks

We consider the time-harmonic scattering problem in the resonance frequencies. Let Γ be any sound-hard crack and take an acoustic incident plane wave of the form

$$u^{inc}(x) = e^{ikx\cdot d},$$

where $d \in S^2$, is an unitary direction that determines the direction of propagation of the acoustic wave with any frequency (or wavenumber) $k > 0$. Here we are interested in the case of resonance frequencies, that can not be dealt with the asymptotic behavior on k, here the wavelength has dimensions comparable to the crack itself.

The scattered wave u verifies the Helmholtz equation, and we have the exterior domain problem

$$\begin{cases} \Delta u + k^2 u = 0 & \text{in } \mathbb{R}^3\backslash\Gamma \\ \partial_n u = -\partial_n u^{inc} & \text{on } \Gamma \\ \partial_r u - iku = o(r^{-1}) & \text{when } r = |x| \to \infty \end{cases}$$

where the last condition is the Sommerfeld radiation condition. It is well known that the behavior of the scattered wave can be described by the asymptotic relation

$$u(x) = \frac{e^{ikr}}{r} u_\infty(\hat{x}) + o(\frac{1}{r})$$

where $\hat{x} = \frac{x}{|x|} \in S^2$, and u_∞ is an analytic function with complex values defined on the unitary sphere S^2, called *far field pattern*.

The solution of this problem can be given in terms of a double layer potential (e.g.[6])

$$u(x) = \int_\Gamma \partial_{n_y} \Phi(x-y)\varphi(y) ds_y, \quad (x \in \mathbb{R}^3\backslash\Gamma) \tag{1}$$

where Φ is the fundamental solution of the Helmholtz equation given by

$$\Phi(x) = \frac{e^{ik|x|}}{4\pi|x|}.$$

and $\varphi \in H_{00}^{1/2}(\Gamma)$ is a density called *crack opening displacement* (COD). This COD is the jump of the solution on Γ, ie. $\varphi = [u] = u^- - u^+$, where u^- and u^+ are the traces of the solution according to a prescribed normal orientation. The effect of this arbitrary orientation is cancelled by the sign of the normal derivative in formula (1).

Remarks:

• Note that the single layer representation presents a problem in the crack situation, since one assumes the same response in both sides of the crack and therefore there is no jump using the traces of the normal derivative. Thus, the unknown density used in single layer formulation, which is given by the jump of the traces of the normal derivative, is not appropriate.

• On the other hand, the trace of the double layer potential is given by

$$-\partial_{n_x} u^{inc}(x) = \partial_{n_x} \int_\Gamma \partial_{n_y} \Phi(x-y)\varphi(y) ds_y, \tag{2}$$

and if one tries to use the collocation method, one should find a way to avoid the hypersingular kernel, since

$$\partial_{n_x}\partial_{n_y}\Phi(x-y) = O(\frac{1}{|x-y|^3})$$

is not integrable in the usual sense.

A way to deal with this problem is to use analytical series developments, that work only for simple geometries (e.g. [9], [10], [12]), to regularize the problem and then use collocation methods (e.g.[11], [4]), or to use variational formulation methods ([7] and [1]) The first numerical results comparing these approaches, in the elastic case, were made in [1], for simple geometries (penny-shaped or elliptical flat cracks, since no other results were available), showing clearly the advantages of the variational formulation (due to the coerciveness of the sesquilinear form). In [1] other geometries were considered, but the implementation of the method was restricted to flat cracks.

However the variational problem on the boundary (cf. Hamdi [8]) also holds for *non flat cracks*, and we must retrieve the density $\varphi \in H_{00}^{1/2}(\Gamma)$ such that

$$\begin{aligned} \int_\Gamma \int_\Gamma \Phi(x-y) \big(& \mathbf{curl}_\Gamma \varphi(x) \cdot \mathbf{curl}_\Gamma \bar{\psi}(y) \\ & -k^2 \mathbf{n}_x(x) \cdot \mathbf{n}_y(y) \varphi(x) \bar{\psi}(y) \big) \, ds_y ds_x \\ = & -\int_\Gamma \partial_n u^{inc}(x) \bar{\psi}(x) ds_x, \end{aligned} \tag{3}$$

for all test functions $\psi \in H_{00}^{1/2}(\Gamma)$. Note that $\mathbf{curl}_\Gamma \varphi$ stands for the surface curl given by

$$\mathbf{curl}_\Gamma \varphi(x) = \mathbf{n}_x \times \nabla \tilde{\varphi}(x),$$

where $\tilde{\varphi}$ is a constant extension of φ along the normal direction. Also, the arbitrary sign of the normal directions $\mathbf{n}_x$ does not affect the sesquilinear formula in (3).

In this way it is possible to avoid the hypersingular kernel, because we only have $\Phi(x-y)$, since the derivatives were transferred to the density and to the test functions. Note that $\nabla\tilde{\varphi}$ is well defined since $\varphi \in H^{1/2}(\Gamma)$ and for regular cracks (with no corners) one can extend it locally into a $\tilde{\varphi} \in H^1(\omega)$, where ω is a 3D-neighborhood of Γ.

We may proceed with the discretization using a finite boundary element method (eg. [1]).

3 Boundary Finite Element Method

The procedure is quite similar to the classical finite element method on 2D. As usual we have to take into account two types of errors. The errors due to the discretization of the geometry and the errors inherent to the approximation by interpolation in a finite dimensional space.

We will consider cracks defined by a regular function on Q, (for simplicity, a square on $\mathbb{R}^2$), i.e.:

$$\Gamma = \{(x^*, f(x^*)), \text{ with } f : Q \to \mathbb{R} \},$$

where $x^* = (x_1, x_2) \in \mathbb{R}^2$. The smoothness of the function f defines the smoothness of the surface Γ, and we will be only dealing with C^1 surfaces, although for the purpose of discretization we will take a piecewise linear surfaces, defined by the triangles

$$T_k = \bigcup_{i=1}^{3} (x^*_{k_i},\ f(x^*_{k_i}))$$

where $x^*_{k_i}$ are points in a 2D triangular mesh defined on Q and k_i stands for the representation in global numeration on the node i in the triangle k.

This way we define a piecewise triangular $\Gamma_h = \cup_k T_k$ surface approximating Γ, where h stands for the maximal diameter of the triangles T_k.

Note that the mesh on Q does not export its properties to Γ_h. For instance, a steep function f may transform a regular triangle τ_k on Q into a huge, or even almost degenerated, triangle $T_k = f(\tau_k)$.

In the regular mesh we consider linear Lagrange finite elements, vanishing on the boundary of Γ_h, therefore these test functions are in the space $H_{00}^{1/2}(\Gamma_h)$.

In Figure 1 we plot an example of triangulation for a non flat crack. Γ (remark that each interior node has six adjacent triangles). This triangulation was based on a regular mesh built on $Q = [-1, 1]^2$ and approaches Γ with an error of $O(h^2)$. Two of the corners are suppressed, to keep the convenient feature of having six adjacent triangles per interior node. The suppression of these two corners has a minimal effect on the approximation, for non steep f, because the function φ vanishes on the border of Γ, and therefore that contribution is not quite significant.

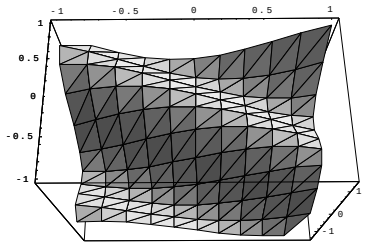

Figure 1. .The mesh on a non flat crack, defined by a function f.

We do not go into further details on the discretization procedure, the reader can find similar techniques in [1], for the case of elastic flat cracks, that can be adapted to this problem. We just mention that the procedure consists in calculating the double integral on the sesquilinear form as the sum of double integrations on the triangles, differentiating two cases:

(i) Non adjacent triangles $\longmapsto$ we consider simple numerical integration in both integrals using interior Gauss points.

(ii) Adjacent triangles $\longmapsto$ we consider a numerical integration on the first integral and an analytical integration of

$$\int_{T_j} \Phi(x - y_i) \left(\mathbf{curl}_\Gamma \varphi(x) \cdot \mathbf{curl}_\Gamma \bar{\psi}(y_i) - k^2 \mathbf{n}_x(x) \cdot \mathbf{n}_y(y_i) \varphi(x) \bar{\psi}(y_i) \right) ds_x$$

here φ and ψ are to be understood as the basis functions, and y_i is a Gauss point on the adjacent triangle. Note that it may be the same and this implies $y_i \in T_j$. In fact, since we are considering interior Gauss points, the only problem arrives when we are integrating on the same triangle. The other adjacent cases may be calculated numerically. Most of the calculation time is spent with the non trivial analytical calculation.

Finally, having φ approached by the linear combination of the basis functions (with coefficients given by the solution of the stiff system), we may calculate an approximation of the far field pattern by the formula

$$u_\infty(\hat{x}) = \frac{1}{4\pi} \int_\Gamma \partial_{n_y} e^{-ik\hat{x}.y} \varphi(y) ds_y,$$

using numerical integration with the basis functions.

4 Numerical tests

We considered simple tests to check the performance of the method. First of all we should state that the results obtained by the method applied for flat cracks like in [1] coincide with the case cracks in arbitrary planes. This was a basic, but essential test, since no other results were available for non flat cracks.

Example 1. We considered an incident plane wave with direction $d = (0, 0, -1)$ and $k = 6$. The crack is given by $f(x_1, x_2) = \frac{1}{2}x_1^2$.

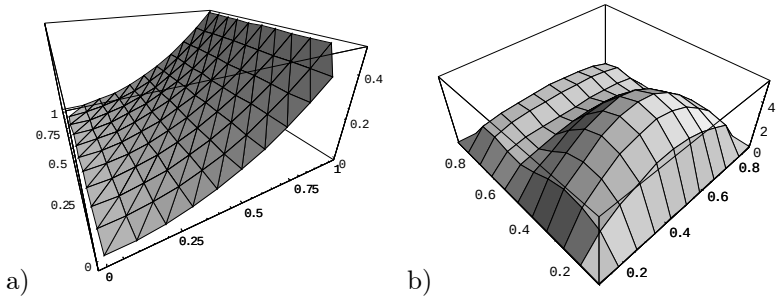

Figure 2. The crack (a) and the COD (b) of Example 1.

In Figure 2.a) we plotted the mesh. We used 81 interior points in $Q = [0, 1]^2$, with $h_Q = 0.1$, noticing that this gives a reasonable system with 81 complex unknowns, but, as pointed out before, most of the computation time is taken on the analytic evaluation of the singular part of the integrals. One should also remark that, in wave scattering, we can not expect a good approximation unless the wavelength is four times bigger than the distance between the nodes, i.e. usually one should take $k < \frac{\pi}{2h}$. In our case, since $h \sim 0.17$, the value $k = 6$ is inside the limit of this empiric criteria. In Figure 2.b) we plotted the modulus value for the COD, in each interior node, i.e. we plotted the list of $|\varphi(x_i)|$.

In Figure 3, we plotted two different 3D views of the far field pattern generated by the scattered wave. These pictures were made using the *ListSurfacePlot3D* routine of *Mathematica*©, based on an adequate list of values given by our Fortran 90 code. We plotted the absolute values of the far field, i.e. $|u_\infty(\hat{x})|$, for 36×36 points on the surface of the unitary sphere. We may notice the big lobs produced by the reflection and refraction of the wave on the crack. The refraction lob is similar to the one that we have in the flat cracks situation, but a similar reflection lob is no longer present. The reflection lob seems to be more affected by the shape of the crack, and we remark the presence of oblique lobs that agrees with geometric ray simplification for high frequencies.

We also would like to mention that in this situation we no longer have null far field cuts. This was a particular feature of plane crack scattering.

As it was proved in [2] and [3], the null far field cuts are a unique feature of cracks and they allow to identify the plane of the crack. However one notices small far field values in a possible plane approximation of the crack, as expected.

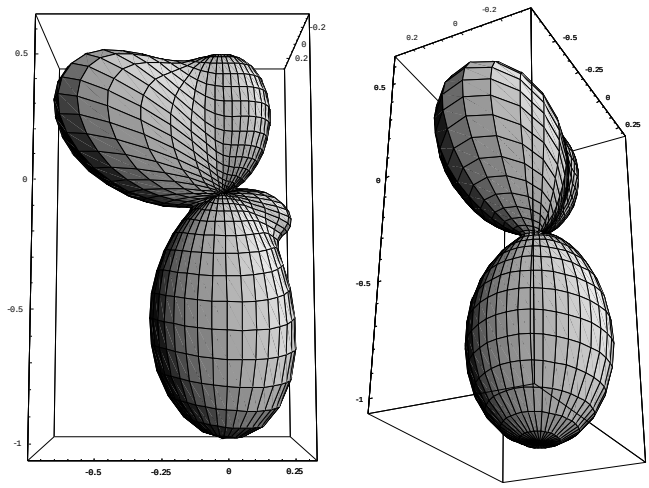

Figure 3. Two different views of the far field pattern of Example 1.

Example 2.

We considered a crack defined on $Q = [-1, 1]\times[-0.5, 0.5]$ and $f(x_1, x_2) = x_1x_2$ and a plane incident wave with $d = \frac{1}{\sqrt{2}}(-1, 0, -1)$.

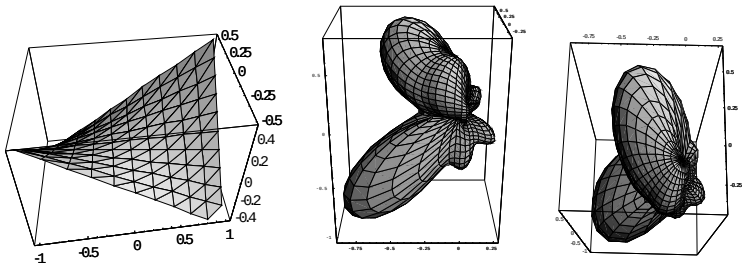

Figure 4. Mesh of the crack and two views of the far field pattern (data from Example 2).

In Figure 4 we plot the mesh and two views of the far field pattern, using the same $k = 6$, and the same number of nodes as in Example 1. With this incidence direction, we may see that the far field pattern has an influence of the ray trajectories and it is also influenced by the curvatures

of the crack (see the last picture in Figure 4). The far field pattern is much more complex in the case of non flat cracks, which is perfectly natural since it should follow the geometry of the shape. Note that it is this feature that allows the identification of the crack using inverse problem techniques.

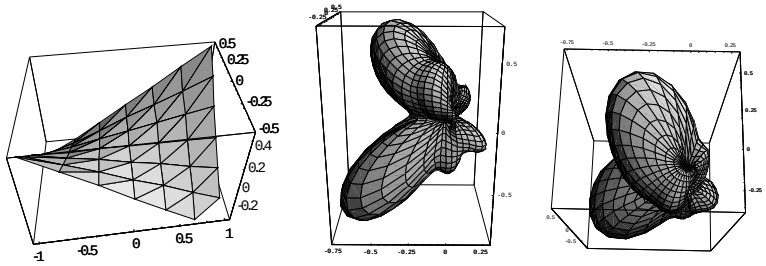

Figure 5. The same tests as in Figure 4 but considering a larger h (results are almost identical).

If in Figure 4 we took a mesh with 81 interior points, which gave $h \sim 0.27$, now, in Figure 5, we plot the same experiment for less points. We took 25 interior points, corresponding to $h \sim 0.47$. As one may see the results are almost identical in visual terms. This puts out the good behavior of the boundary variational formulation method using finite elements, in convergence tests.

4.1 Convergence Tests

In Figure 6 we plotted the convergence test for the crack and data prescribed in Example 1.

We took for approximations

- 9 interior points, with $h = 0.42$ (dashed thin line),
- 25 interior points, with $h = 0.28$ (thin line),
- 49 points, with $h = 0.21$ (dashed thick line),
- 81 points, with $h = 0.17$ (thick line)

We can clearly see the good convergence rate of the approximations. Even the first approximation gives a good portrait of the global behavior of the solution. Of course, if one wants to get detailed profiles, then the number of points must be increased. This somehow agrees with a possible rough approximation of the shape of the crack using a regularization of a noisy far field pattern data. In fact, one may see the far field generated by this rough approximation as the consequence of regularizing noise that was

added to the far field of the original shape.

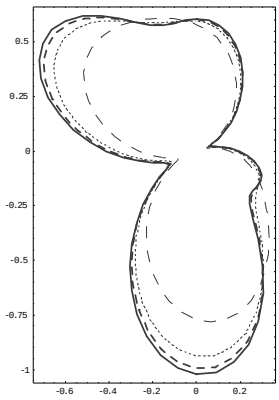

Figure 6. Convergence test for Example 1.

In Figure 7 we present the same test, with the single difference that we used $k = 9$ and an incidence direction $d = (\frac{1}{2}, 0, \frac{-\sqrt{3}}{2})$. The considerations made for the previous case also apply here - mainly, there is a good convergence rate. Moreover, we can see that there is a connection between small values of the far field pattern and a possible plane approximation to the non planar crack, since the shape of the crack could be roughly approximated by the plane defined by $x_3 = \frac{1}{2}x_1 - \frac{1}{12}$ and it is in this direction that the cut of the far field presents the smaller absolute values.

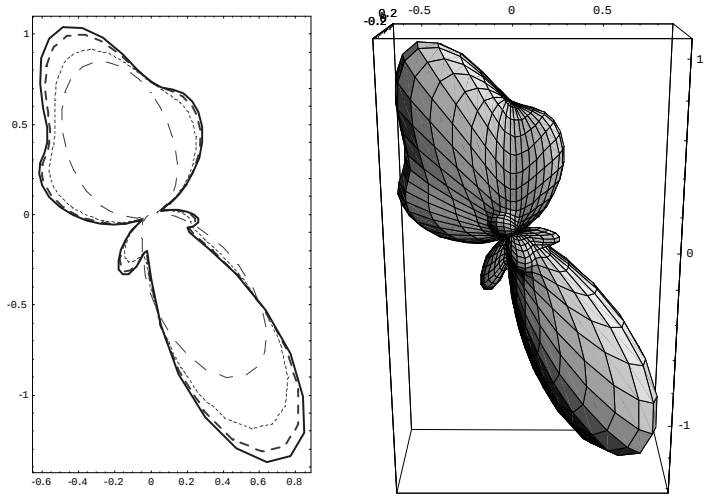

Figure 7. Convergence test for Example 1 with different data and the associated 3D plot.

• **Conclusions**

We may conclude that a good way of formulating the crack scattering problem in terms of the double layer potential with continuous Neumann data on both sides of the boundary is to use a variational formulation on the surface and afterwards to apply a numerical resolution using a boundary finite element method on the crack surface. This provides an excellent method to avoid the hypersingularity which is also stable and converges fast. Moreover rough approximations with a small number of points allow a fairly good preview of the global behavior of the far field pattern. Applications to crack detection follow from the works in [1], [2] and more generally using the methods described in [6]. An extension of this code to the elastic crack situation is currently being made.

Acknowledgments**:** This work was partially supported by FCT, Project POCTI/ MAT/ 34735/ 99/00.

References

[1] Alves C. J. S.; Ha Duong T.: Numerical resolution of the boundary integral equations for elastic scattering by a plane crack, *Int J. Num. Meth. Eng.*, **38**, pp.2347-2371, 1995

[2] Alves C. J. S.; Ha Duong T.: On inverse scattering by screens, *Inverse Problems*, **13**, pp.1161-1176, 1997

[3] Alves C. J. S.; Ribeiro P.M.C.: Crack detection using spherical waves and near field measurements, *in Advances in Boundary Elements (Ed: C. Brebbia, H. Power)*, WIT Press, pp.335-344, 1999

[4] Bonnet, M.: Regularized BIE formulations for first- and second-order shape sensitivity of elastic fields. *Comput. & Structures* **56,** pp.799–811, 1995.

[5] Bouwkamp, C. J.: Diffraction theory. *Reports on Progress in Physics* **17**, pp.35–100, 1954.

[6] Colton D., Kress R.: Inverse acoustic and electromagnetic scattering theory, *Springer-Verlag,* 2nd. ed., 1998

[7] Ha Duong, T.: On the boundary integral equations for the crack opening displacement of flat cracks, *Int. Eq. Op. Th.*, pp.427-453, 1992

[8] Hamdi, M. A.: Une formulation variationnelle par équations intégrales pour la résolution de l'équation de Helmholtz avec des conditions aux limites mixtes, *C.R.A.S.*II **292**, pp.17–20, 1981.

[9] Jones, D. S.: A new method for calculating scattering with particular reference to the circular disc. *Comm. Pure Appl. Math.* **9**, pp.713–746, 1956.

[10] Martin, P. A.; Wickham, G. R.: Diffraction of elastic waves by a penny-shaped crack: analytical and numerical results. *Proc. Roy. Soc. Lond.,* **A 390**, pp 91–129, 1983.

[11] Martin, P. A.; Rizzo, F. J.: On boundary integral equations for crack problems. *Proc. Roy. Soc. Lond.*, **A 421**, pp.341–355, 1989

[12] Penzel, F.: Mixed Fourier boundary element methods for computing time-harmonic scattering fields on screens, *Math. Nachr.* **175,** pp.269–324, 1995.